Title	Relaxation of a Free-Molecular Gas to Equilibrium Caused by Interaction with Vessel Wall
Author(s)	Tsuji, Tetsuro; Aoki, Kazuo; Golse, François
Citation	Journal of Statistical Physics (2010), 140(3): 518-543
Issue Date	2010-08
URL	http://hdl.handle.net/2433/126618
Right	The original publication is available at www.springerlink.com
Type	Journal Article
Textversion	author

Noname manuscript No.
(will be inserted by the editor)

Tetsuro Tsuji · Kazuo Aoki · François Golse

Relaxation of a free-molecular gas to equilibrium caused by interaction with vessel wall

Received: date / Accepted: date

Abstract A free-molecular gas contained in a static vessel with a uniform temperature is considered. The approach of the velocity distribution function of the gas molecules from a given initial distribution to the uniform equilibrium state at rest is investigated numerically under the diffuse reflection boundary condition. This relaxation is caused by the interaction of gas molecules with the vessel wall. It is shown that, for a spherical vessel, the velocity distribution function approaches the final uniform equilibrium distribution in such a way that their difference decreases in proportion to an inverse power of time. This is slower than the known result for a rarefied gas with molecular collisions.

Keywords Free-molecular gas · Approach to equilibrium · Diffuse reflection · Kinetic theory of gases

PACS 05.20.Dd · 47.45.Dt · 51.10.+y · 47.45.Ab · 47.45.-n

T. Tsuji
Department of Mechanical Engineering and Science
Kyoto University, Kyoto 606-8501, Japan
E-mail: t.tsuji@ft2.ecs.kyoto-u.ac.jp

K. Aoki
Department of Mechanical Engineering and Science
and Advanced Research Institute of Fluid Science and Engineering
Kyoto University, Kyoto 606-8501, Japan
E-mail: aoki@aero.mbox.media.kyoto-u.ac.jp

F. Golse
Centre de Mathématiques Laurent Schwartz
École Polytechnique
91128, Palaiseau cedex, France
E-mail: golse@math.polytechnique.fr

1 Introduction

Let us consider an ideal rarefied gas contained in a vessel kept at a uniform temperature. In the absence of gravity, the steady state of the gas is uniform equilibrium at rest at the same temperature as the vessel. If the equilibrium is perturbed, the state of the gas approaches the equilibrium as time goes on. In the present paper, we are concerned with this approach.

When the mean free path of the gas molecules is not negligibly small compared with the size of the vessel, continuum fluid dynamics is not valid, and we need to use kinetic theory to describe the above-mentioned approach to equilibrium. That is, it is described by the Boltzmann equation with its initial and boundary conditions. It is intuitively clear that the velocity distribution function of the gas molecules, starting from a given initial distribution, approaches the global stationary Maxwellian distribution with a density given by the average density of the initial distribution and with the same temperature as the vessel, which we call the *final equilibrium state*. However, rigorous mathematical study concerning the above statement is relatively recent [1–3].

In recent years, the rate of approach to the final equilibrium state has been an important subject of mathematical study of the Boltzmann equation [4–9]. In [8], the following result is reported. Let t_* be the time variable, f_* the velocity distribution function of the gas molecules, and M_{w*} the final equilibrium distribution. If the boundary condition on the vessel wall is diffuse reflection, then, it holds that

$$\|f_* - M_{w*}\| = O(t_*^{-\delta}), \quad \text{as} \ \ t_* \to \infty, \tag{1}$$

with any positive number δ, where $\|\cdot\|$ is a suitably defined norm. The rapid decay (1) is also true for some different types of boundary condition on the vessel wall, such as the specular-reflection and periodic conditions [4,5]. However, for these boundary conditions, the temperature of the final equilibrium state is determined by the initial condition. It should be mentioned that exponential decay was recently proved [9] for the above-mentioned boundary conditions with stronger mathematical results in the case where the solution is close to the final equilibrium state (see also [10,11] for the periodic condition).

The approach to equilibrium is caused by two factors:

(i) Collisions between gas molecules.
(ii) Interaction between gas molecules and the vessel wall.

The effect of factor (ii) is absent for the specular-reflection and periodic boundary conditions.

Now let us consider the case where the gas is so rarefied that the interaction between the gas molecules is neglected. Such a gas is called the free-molecular gas or the Knudsen gas, characterized by infinitely large Knudsen number (the mean free path of the gas molecules divided by the characteristic length of the vessel). In this case, the approach to the final equilibrium state is caused only by factor (ii). Therefore, the manner of approach may depend on the type of interaction between the gas molecules and the vessel wall, i.e., the boundary condition of the Boltzmann equation, as well as the

shape and space dimension of the vessel. In fact, if the initial distribution is not an equilibrium state, the gas never approaches the final equilibrium state for specular reflection and for the periodic condition, since these conditions have no thermalizing effect. Furthermore, even for the boundary conditions with thermalizing effect, the thermalization takes place non-uniformly in the molecular velocity space. That is, fast molecules hit the boundary and are thermalized quickly, whereas it takes a long time for slow molecules to interact with the boundary. The non-uniform convergence of the velocity distribution function in the molecular velocity space may cause a slow approach of the velocity-averaged (or macroscopic) quantities to their equilibrium values.

The approach to the final equilibrium state for a free-molecular gas is a special case of the approach to the stationary solution when the wall temperature is not uniform. The latter problem has been studied by several authors: for instance, [3] for the diffuse reflection condition in the three-dimensional (3D) setting, [12,13] for a more general boundary condition in the one-dimensional (1D) setting, and [14] for a discrete-velocity model in the 1D setting. In these works, however, the rate of approach has not been discussed. To the best of the authors' knowledge, an exception is the recent work by Yu [15], in which an interesting probabilistic method was developed for the approach to the stationary solution in the 1D setting (in a slab) for diffuse reflection. He was able to give detailed estimates for the rate of the non-uniform convergence of the velocity distribution function mentioned above. However, the optimal rate of approach to the final equilibrium state, which is comparable with Eq. (1), has not yet been found. In this connection, we should also refer to a recent paper by Desvillettes and Salvarani [16], which investigates the decay rate for a simple transport equation with a collision term vanishing in a certain space domain.

In the present study, we investigate numerically the same problem (the approach of a free-molecular gas to the final equilibrium state). We consider a free-molecular gas in a vessel with a uniform temperature, on the wall of which the gas molecules undergo diffuse reflection. We restrict ourselves to a vessel of spherical shape of dimension d, i.e., a sphere for the 3D case ($d = 3$), a circular cylinder for the 2D case ($d = 2$), and a gap between two parallel plates for the 1D case ($d = 1$). In addition, we are mainly concerned with the spherically symmetric case with a special initial condition, i.e., a uniform equilibrium state at rest with a (finite) temperature different from that of the vessel. These restrictions make the computation for the 2D and 3D cases feasible. We will investigate the decay rate to the final equilibrium state of the velocity distribution function as well as the macroscopic quantities. As a result, we will give numerical evidence that the decay is in proportion to an inverse power of time, for instance,

$$\|f_* - M_{w*}\| \approx C^{(d)}/t_*^d, \qquad (d = 1,\ 2,\ 3), \tag{2}$$

as $t_* \to \infty$, where $\|\cdot\|$ is a kind of L^1 norm in the position and molecular velocity, and $C^{(d)}$ are positive constants.

2 Formulation of the problem

2.1 Problem, assumptions, and notations

Consider a rarefied monatomic gas in a vessel kept at a uniform and constant temperature T_{w*}. If the state of the gas is given at initial time $t_* = 0$, then it evolves in time and approaches the final equilibrium state, i.e., the uniform equilibrium state at rest with temperature T_{w*} and density equal to the average density of the initial state. We investigate the process of approach numerically, with special interest in the asymptotic behavior of the gas, under the following assumptions:

(i) The behavior of the gas is described by the Boltzmann equation.
(ii) The gas is so rarefied that the effect of collisions between the gas molecules is negligible (free-molecular or Knudsen gas).
(iii) The interaction between the gas molecules and the vessel wall is described by diffuse reflection. That is, the gas molecules leaving the wall are distributed according to the stationary Maxwellian distribution with temperature T_{w*}, and the condition of no net mass flux across the wall is satisfied.
(iv) The vessel is of spherical shape of dimension d with diameter L. To be more specific, the vessel is a sphere of diameter L for $d = 3$, a circular cylinder of diameter L for $d = 2$, and a gap of width L between two parallel plates for $d = 1$.

Let ρ_{0*} be the average density of the gas associated with the initial velocity distribution function. Then, the final equilibrium distribution M_{w*} is given by

$$M_{w*} = \frac{\rho_{0*}}{(2\pi R T_{w*})^{3/2}} \exp\left(-\frac{\xi_i^2}{2RT_{w*}}\right), \tag{3}$$

where ξ_i is the molecular velocity, and R is the gas constant per unit mass ($R = k/m$ with k the Boltzmann constant and m the mass of a molecule). We take

$$L, \quad T_{w*}, \quad \rho_{0*}, \quad c_{w*} = (2RT_{w*})^{1/2}, \quad t_{w*} = L/c_{w*}, \tag{4}$$

as the reference length, temperature, density, velocity, and time, respectively. Let X_i be the Cartesian coordinates in space, t_* the time variable (as already appeared), $f_*(X_i, \xi_i, t_*)$ the velocity distribution function of the gas molecules, $\rho_*(X_i, t_*)$ the density of the gas, $u_{i*}(X_i, t_*)$ the flow velocity, and $T_*(X_i, t_*)$ the temperature. Then, we introduce the dimensionless counterparts $[x_i, t, \zeta_i, f, M_w, \rho, u_i, T]$ of $[X_i, t_*, \xi_i, f_*(X_i, \xi_i, t_*), M_{w*}, \rho_*(X_i, t_*), u_{i*}(X_i, t_*), T_*(X_i, t_*)]$ by the following relations:

$$\begin{aligned} &X_i = Lx_i, \qquad t_* = t_{w*}t, \qquad \xi_i = c_{w*}\zeta_i, \\ &f_* = (\rho_{0*}/c_{w*}^3)\, f, \qquad M_{w*} = (\rho_{0*}/c_{w*}^3)\, M_w, \\ &\rho_* = \rho_{0*}\rho, \qquad u_{i*} = c_{w*}u_i, \qquad T_* = T_{w*}T. \end{aligned} \tag{5}$$

We suppose that the spherical vessel (of dimension d) is given by $S_d(x_i) = 0$ ($d = 1, 2, 3$) in the dimensionless x_i space and its inside (the region of the gas) is described by $\mathcal{D} = \{ x_i \,|\, S_d(x_i) < 0 \}$. That is,

$$S_1(x_1) = x_1^2 - \frac{1}{4}, \tag{6a}$$

$$S_2(x_1, x_2) = x_1^2 + x_2^2 - \frac{1}{4}, \tag{6b}$$

$$S_3(x_1, x_2, x_3) = x_1^2 + x_2^2 + x_3^2 - \frac{1}{4}. \tag{6c}$$

In addition, $n_i(x_i) = -\nabla S_d / |\nabla S_d|$ denotes the unit normal vector to the surface of the vessel pointed toward the gas.

2.2 Basic equation

The (dimensionless) Boltzmann equation for a free-molecular gas reads

$$\frac{\partial f}{\partial t} + \zeta_i \frac{\partial f}{\partial x_i} = 0, \tag{7}$$

which is the so-called free transport equation. The corresponding initial condition is given by

$$f(x_i, \zeta_i, 0) = f_0(x_i, \zeta_i), \tag{8}$$

and the boundary condition (diffuse reflection) on the vessel wall by

$$f(x_i, \zeta_i, t) = f_w(x_i, \zeta_i, t), \qquad \text{for } S_d(x_i) = 0,\ \zeta_i n_i > 0, \tag{9a}$$

$$f_w(x_i, \zeta_i, t) = \rho_w(x_i, t) M_w(\zeta_i), \tag{9b}$$

$$\rho_w(x_i, t) = -2\pi^{1/2} \int_{\zeta_j n_j < 0} \zeta_j n_j f(x_i, \zeta_i, t) \mathrm{d}\boldsymbol{\zeta}, \tag{9c}$$

where $\mathrm{d}\boldsymbol{\zeta} = \mathrm{d}\zeta_1 \mathrm{d}\zeta_2 \mathrm{d}\zeta_3$, and M_w is the dimensionless reference Maxwellian (i.e., the dimensionless final equilibrium distribution), i.e.,

$$M_w(\zeta_i) = \pi^{-3/2} \exp(-\zeta_i^2). \tag{10}$$

Here, we exclude the initial condition f_0 with the concentration of mass at $\zeta_i = 0$ (e.g., f_0 containing the Dirac delta centered at $\zeta_i = 0$).

The density ρ, flow velocity u_i, and temperature T are defined as the following moments of f:

$$\rho(x_i, t) = \int f \mathrm{d}\boldsymbol{\zeta}, \tag{11a}$$

$$u_i(x_i, t) = \frac{1}{\rho} \int \zeta_i f \mathrm{d}\boldsymbol{\zeta}, \tag{11b}$$

$$T(x_i, t) = \frac{2}{3\rho} \int (\zeta_i - u_i)^2 f \mathrm{d}\boldsymbol{\zeta}, \tag{11c}$$

where, and in Eqs. (12) and (13) below, the domain of integration is the whole space of ζ_i (or ξ_i). In addition, we introduce the (dimensionless) relative entropy $W(f|M_w)$:

$$W(f|M_w) = \int f \ln(f/M_w) \mathrm{d}\boldsymbol{\zeta}, \tag{12}$$

the dimensional counterpart of which is given as

$$W_*(f_*|M_{w*}) = \rho_{0*} W(f|M_w) = \int f_* \ln(f_*/M_{w*}) \mathrm{d}\boldsymbol{\xi}. \tag{13}$$

As time goes on, f approaches the final equilibrium state M_w except at $\zeta_i = 0$. Thus, we have

$$\lim_{t\to\infty} \rho_w(x_i, t) = 1, \tag{14}$$

and

$$\begin{aligned} &\lim_{t\to\infty} \rho(x_i, t) = 1, \quad \lim_{t\to\infty} u_i(x_i, t) = 0, \\ &\lim_{t\to\infty} T(x_i, t) = 1, \quad \lim_{t\to\infty} W(f|M_w) = 0. \end{aligned} \tag{15}$$

The fact that f approaches the unique limit M_w is intuitively obvious for a vessel of arbitrary shape. However, its mathematical proof is relatively recent [1,3].

When f_* is a local Maxwellian distribution, W_*/ρ_* reduces to $\ln(\rho_*/\rho_{0*}) - (3/2)\ln(T_*/T_{w*}) + (3/2)(T_*/T_{w*}) + \text{const}$, which can be expressed as $(e_* - T_{w*}s_*)/RT_{w*} + \text{const}$, where e_* and s_* are the internal energy and entropy per unit mass, respectively. Since $F_* = e_* - T_* s_*$ is the Helmholtz free energy per unit mass, W_* is similar to it. In particular, F_* for $\rho_* = \rho_{0*}$ and $T_* = T_{w*}$ corresponds to $W_* = 0$. Let us denote by $\langle W \rangle$ the integral of W over the vessel, i.e.,

$$\langle W \rangle = \int_{\mathcal{D}} W \mathrm{d}\mathbf{x}, \tag{16}$$

with $\mathrm{d}\mathbf{x} = \mathrm{d}x_1 \mathrm{d}x_2 \mathrm{d}x_3$ and with the obvious interpretation in the 1D and 2D cases. Then, we can show, from Eqs. (7) and (9), that $\mathrm{d}\langle W \rangle/\mathrm{d}t \le 0$ and the equality sign holds if and only if $f = M_w$ (i.e., $W = 0$). This fact is consistent with the Helmholtz potential minimum principle in thermodynamics [17]. Since $\langle W \rangle$ has been used as a measure of deviation of f from M_w (e.g., [4–6, 8, 12]), we also use it for the same purpose.

3 Preliminaries

In this section, we carry out some preliminary analyses for the numerical analysis. The solution of the free transport equation (7) is expressed as

$$f(x_i, \zeta_i, t) = f(x_i - \zeta_i(t-s), \zeta_i, s), \qquad (0 \le s \le t). \tag{17}$$

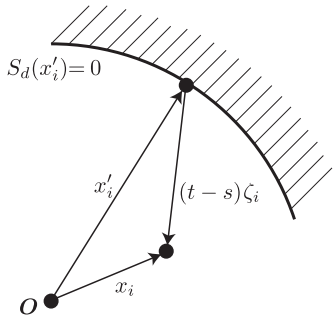

Fig. 1 Configuration. The relation between x_i in the gas and x_i' on the vessel wall in terms of the present time t, the time in the past s, and the molecular velocity ζ_i.

That is, the velocity distribution function is constant along the trajectory of a molecule in $(x_i,\, t)$ space. Therefore, one can obtain information on the velocity distribution function by tracing back the trajectories of the molecules. If we trace back, from a given point $(x_i,\, t)$ in $(x_i,\, t)$ space, the trajectory of a molecule with a given velocity ζ_i, we either reach the initial time $t = 0$ without hitting the vessel wall, or hit the wall at time s in the past. The time s, which is a function of x_i, ζ_i, and t, is obtained as follows.

Since the molecule with velocity ζ_i that left the vessel wall at time s reaches the position x_i at time t, the following relation holds (see Fig. 1).

$$x_i' = x_i - (t-s)\zeta_i, \qquad S_d(x_i') = 0. \tag{18}$$

Solving these equations for s, we obtain the departure time $s(x_i,\, \zeta_i,\, t)$ together with the departure point x_i'. If $s(x_i,\, \zeta_i,\, t)$ is negative, this means that the trajectory can be traced back to the initial time without hitting the vessel wall. In such a case, the value of $f(x_i,\, \zeta_i,\, t)$ is given by the initial condition $f_0(x_i,\, \zeta_i)$.

From these facts, we can write the solution of the initial and boundary value problem (7)–(9) formally in the following form:

$$f(x_i,\, \zeta_i,\, t) = f_0(x_i - \zeta_i t,\, \zeta_i), \quad \text{for} \quad \zeta_i \in \Omega_0(x_i,\, t), \tag{19a}$$

$$\begin{aligned} f(x_i,\, \zeta_i,\, t) &= f_w(x_i - \zeta_i(t-s),\, \zeta_i,\, s) \\ &= \rho_w(x_i - \zeta_i(t-s),\, s) M_w(\zeta_i), \quad \text{for} \quad \zeta_i \in \Omega_w(x_i,\, t), \end{aligned} \tag{19b}$$

where Ω_0 is the set of ζ_i for which Eq. (18) gives a negative solution s $(s < 0)$, and Ω_w the set of ζ_i for which Eq. (18) gives a non-negative solution $(0 \le s \le t)$; s in Eq. (19b) is the non-negative solution $s(x_i,\, \zeta_i,\, t)$ of Eq. (18), i.e.,

$$S_d\Big(x_i - \zeta_i[t - s(x_i,\, \zeta_i,\, t)] \Big) = 0, \qquad 0 \le s(x_i,\, \zeta_i,\, t) \le t. \tag{20}$$

[See the next paragraph for the explicit form of $s(x_i,\, \zeta_i,\, t)$.] Since f_0 is given, we have the solution if ρ_w is found. Substitution of Eq. (19) into Eq. (9c) yields the following integral equation for ρ_w:

$$\frac{\rho_w(x_i,\, t)}{2\sqrt{\pi}} = -\int_{\substack{\zeta_j n_j < 0 \\ \zeta_i \,\in\, \Omega_0(x_i,\, t)}} \zeta_j n_j f_0(x_i - \zeta_i t,\, \zeta_i)\, \mathrm{d}\boldsymbol{\zeta} - \int_{\substack{\zeta_j n_j < 0 \\ \zeta_i \,\in\, \Omega_w(x_i,\, t)}} \zeta_j n_j M_w(\zeta_i)\, \rho_w(x_i - \zeta_i(t-s),\, s)\, \mathrm{d}\boldsymbol{\zeta}, \quad \text{for} \quad S_d(x_i) = 0, \tag{21}$$

where s is given by Eq. (20). Once ρ_w is obtained from Eq. (21), one obtains f from Eq. (19) and then the macroscopic quantities from Eqs. (11) and (12).

Equation (18) yields the following explicit expressions for $s(x_i,\, \zeta_i,\, t)$, $\Omega_0(x_i,\, t)$, and $\Omega_w(x_i,\, t)$ for the three-dimensional case ($d = 3$).

$$s(x_i,\, \zeta_i,\, t) = t - \frac{\zeta_j x_j}{\zeta_k^2} - \frac{1}{\zeta_k^2}\Big[(\zeta_j x_j)^2 - \zeta_k^2\Big(x_l^2 - \frac{1}{4}\Big)\Big]^{1/2}, \tag{22a}$$

$$\Omega_0(x_i,\, t) = \Big\{\, (\zeta_1,\, \zeta_2,\, \zeta_3) \;\Big|\; \Big(\zeta_j - \frac{x_j}{t}\Big)^2 < \frac{1}{4t^2} \,\Big\}, \tag{22b}$$

$$\Omega_w(x_i,\, t) = \Big\{\, (\zeta_1,\, \zeta_2,\, \zeta_3) \;\Big|\; \Big(\zeta_j - \frac{x_j}{t}\Big)^2 \geq \frac{1}{4t^2} \,\Big\}. \tag{22c}$$

The corresponding results for the two- and one-dimensional cases ($d = 2$ and 1) are omitted here.

4 Numerical analysis

This section is devoted to the description of the numerical solution method. We first describe the solution method for the integral equation (21) for ρ_w and then comment on the computation of the macroscopic quantities.

4.1 Integral equation

4.1.1 Special choice of initial condition and simplification

At this point, we consider, as the initial condition, the stationary Maxwellian distribution with temperature T_{0*} and density ρ_{0*}, namely, a uniform equilibrium state at rest with a temperature different from that of the vessel. Thus, its dimensionless form is given by

$$f_0(\zeta_i) = T_0^{-3/2}\, M_w(\zeta_i / T_0^{1/2}), \tag{23a}$$

$$T_0 = T_{0*}/T_{w*}, \tag{23b}$$

where $M_w(\zeta_i)$ is given in Eq. (10). Since the vessel is spherically symmetric, the initial condition (23), which is uniform in x_i and isotropic in ζ_i, yields a solution ρ_w of Eq. (21) that is independent of the position on the vessel wall:

$$\rho_w = \rho_w(t). \tag{24}$$

This fact can be seen from Eq. (21) with the explicit form of $s(x_i, \zeta_i, t)$, $\Omega_0(x_i, t)$, and $\Omega_w(x_i, t)$. It should be noted that the same is true for any spherically symmetric initial conditions. The case of a non-symmetric initial condition will be investigated for the one-dimensional problem ($d = 1$) in Sec. 6.

In these circumstances, Eq. (21) is simplified drastically and is reduced to the following integral equation:

$$\rho_w(t) = M_d(t) + \int_0^t k_d(t-s)\rho_w(s)\mathrm{d}s, \qquad (d = 1, 2, 3). \tag{25}$$

Here

$$\begin{aligned} M_1(t) &= \sqrt{T_0}\Big[1 - \exp\Big(-\frac{1}{T_0 t^2}\Big)\Big], \\ k_1(t) &= \frac{2}{t^3}\exp\Big(-\frac{1}{t^2}\Big), \end{aligned} \tag{26}$$

for $d = 1$,

$$\begin{aligned} M_2(t) &= -\frac{\sqrt{\pi}}{t}\bar{I}_1\Big(-\frac{1}{2T_0 t^2}\Big), \\ k_2(t) &= \frac{\sqrt{\pi}}{t^4}\Big[\bar{I}_0\Big(-\frac{1}{2t^2}\Big) + (1+t^2)\bar{I}_1\Big(-\frac{1}{2t^2}\Big)\Big], \end{aligned} \tag{27}$$

for $d = 2$, and

$$\begin{aligned} M_3(t) &= \sqrt{T_0}\Big[1 - 2T_0 t^2 + (1 + 2T_0 t^2)\exp\Big(-\frac{1}{T_0 t^2}\Big)\Big], \\ k_3(t) &= 4t - \Big(4t + \frac{4}{t} + \frac{2}{t^3}\Big)\exp\Big(-\frac{1}{t^2}\Big), \end{aligned} \tag{28}$$

for $d = 3$; $\bar{I}_n(y)$ in Eq. (27) is defined as

$$\bar{I}_n(y) = \exp(y) I_n(y), \tag{29a}$$

$$I_n(y) = \frac{1}{\pi}\int_0^\pi \cos(n\theta)\exp(y\cos\theta)\mathrm{d}\theta, \tag{29b}$$

where $I_n(y)$ is the modified Bessel function of the first kind of order n. The kernel functions $k_d(t)$ are shown in Fig. 2. As is seen easily, $M_d(t)$ and $k_d(t)$ decay as

$$M_d(t) \approx C_M^{(d)}/t^{d+1}, \qquad k_d(t) \approx C_k^{(d)}/t^{d+2}, \tag{30}$$

as $t \to \infty$, where $C_M^{(d)}$ and $C_k^{(d)}$ are positive constants. In addition, the following relation holds:

$$\int_0^\infty k_d(t)\mathrm{d}t = 1. \tag{31}$$

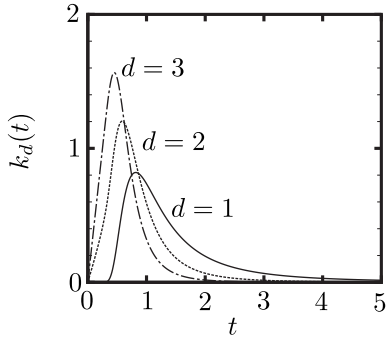

Fig. 2 The kernel functions $k_d(t)$ versus t for $d = 1, 2, 3$. The solid line indicates $k_1(t)$, the dotted line $k_2(t)$, and the dot-dashed line $k_3(t)$.

With the initial condition (23) and thus with Eq. (24), Eq. (19) reduces to a spherically symmetric solution. More specifically, for $d = 1$, $f = f(x_1, \zeta_1, \zeta_t, t)$ with $\zeta_t = (\zeta_2^2+\zeta_3^2)^{1/2}$, satisfying the condition $f(x_1, \zeta_1, \zeta_t, t) = f(-x_1, -\zeta_1, \zeta_t, t)$ (symmetric with respect to the plane $x_1 = 0$ and without a flow parallel to the vessel wall); for $d = 2$, $f = f(\bar{r}, \zeta_{\bar{r}}, |\zeta_{\bar{\theta}}|, |\zeta_3|, t)$, where $(\bar{r}, \bar{\theta}, x_3)$ is the cylindrical coordinate system with $\bar{r} = (x_1^2 + x_2^2)^{1/2}$, and $\zeta_{\bar{r}}$ and $\zeta_{\bar{\theta}}$ are the $\bar{r}$ and $\bar{\theta}$ components of ζ_i (cylindrically symmetric and without axial or circumferential flow); for $d = 3$, $f = f(r, \zeta_r, \zeta_\perp, t)$ with $\zeta_\perp = (\zeta_\theta^2 + \zeta_\varphi^2)^{1/2}$, where (r, θ, φ) is the spherical coordinate system with $r = (x_i^2)^{1/2}$, and ζ_r, ζ_θ, and ζ_φ are, respectively, the r, θ, and φ components of ζ_i.

In the practical computation, in order to reduce the cancellation error, we analyze the following equation for $U(t) = \rho_w(t) - 1$, which vanishes as $t \to \infty$ [see Eq. (14)], rather than Eq. (25):

$$U(t) = M_d(t) - M_d(t)\Big|_{T_0=1} + \int_0^t k_d(t-s)U(s)\mathrm{d}s. \tag{32}$$

The main purpose of the present study is to clarify the asymptotic behavior of the solution as $t \to \infty$. This means that we have to obtain very small values of $U = \rho_w - 1$ with extremely high accuracy for a very long time. In general, such a computation is formidable for the three-dimensional case and is very hard even for the two-dimensional case. Thanks to the initial condition (23), the integral equation for ρ_w has been reduced to the one-dimensional equation (25) or (32) irrespective of the dimension of the spherical vessel. This makes the two- and three-dimensional problems tractable, without harming the two and three dimensionality inherent to the problems.

4.1.2 Numerical method

Numerical analysis of the integral equation (32) is straightforward and simple. Let Δt be the time step, $t_n = n\Delta t$ ($n = 0, 1, 2, ...$) the discretized time

variable, and $U_n = U(t_n)$. If the integral in Eq. (32) at $t = t_n$ is approximated in terms of U_m as

$$\sum_{m=0}^{n} A_m U_m, \tag{33}$$

where A_m depends on the quadrature for the numerical integration, then Eq. (32) at $t = t_n$ gives

$$U_n = \left[M_d(t_n) - M_d(t_n)\Big|_{T_0=1} + \sum_{m=0}^{n-1} A_m U_m \right] (1 - A_n)^{-1}. \tag{34}$$

The sequence $\{U_n\}$ ($n = 0, 1, 2, ...$) is determined by Eq. (34), and we suppose that U_n thus obtained is an approximate solution of $U(t)$ at $t = t_n$.

For the 1D case ($d = 1$), we use the simple trapezoidal rule to determine A_m in Eq. (33). For the 2D and 3D cases ($d = 2, 3$), we approximate $U(t)$ for $t \in [t_{m-1}, t_m]$ by the linear function, i.e., $U(t) \approx (U_m - U_{m-1})(t - t_{m-1})/\Delta t + U_{m-1}$, and carry out the integration for each interval $[t_{m-1}, t_m]$ ($m = 1, 2, ..., n$) analytically to obtain A_m in Eq. (33). The explicit form of A_m is omitted here.

4.1.3 Remark

The integral equation (25) is the classical renewal equation (see, e.g., [18, 19]), and the asymptotic behavior of the solution as $t \to \infty$ is studied in [18]. If we apply Theorem 4 in [18] to Eq. (25), we obtain the following estimate

$$|\rho_w(t) - 1| = o(t^{2-d}), \quad \text{as } t \to \infty, \tag{35}$$

for $d = 2$ and 3. The 1D case does not satisfy the condition of the Theorem (the boundedness of the first-order moment of the kernel). In Sec. 5.2.1, our numerical result will show a decay rate (46). Although the estimate (35) is not sharp at all, the decay rate (46) falls in the range expressed by Eq. (35). As for the 1D case, Theorem 2 of [15] gives the estimate

$$|\rho_w(t) - 1| = O(t^{-1/10}), \quad \text{as } t \to \infty. \tag{36}$$

Our numerical result (46) (with $d = 1$) is contained in this range, though it is not sharp enough, too.

4.2 Macroscopic quantities

4.2.1 Preliminaries

Before presenting the method of computation of the macroscopic quantities, we introduce some additional quantities whose numerical results will also be presented in Sec. 5.

We first define the following marginals of f and M_w for the 1D and 2D cases:

$$\widetilde{f}(x_1,\,\zeta_1,\,t) = \int_{-\infty}^{\infty}\int_{-\infty}^{\infty} f\mathrm{d}\zeta_2\mathrm{d}\zeta_3, \tag{37a}$$

$$\widetilde{M_w} = \int_{-\infty}^{\infty}\int_{-\infty}^{\infty} M_w\mathrm{d}\zeta_2\mathrm{d}\zeta_3 = \frac{1}{\sqrt{\pi}}\exp(-\zeta_1^2), \tag{37b}$$

for $d = 1$, and

$$\widetilde{f}^{(2)}(\bar{r},\,\zeta_{\bar{r}},\,|\zeta_{\bar{\theta}}|,\,t) = \int_{-\infty}^{\infty} f\mathrm{d}\zeta_3, \tag{38a}$$

$$\widetilde{M}_w^{(2)} = \int_{-\infty}^{\infty} M_w\mathrm{d}\zeta_3 = \frac{1}{\pi}\exp(-\zeta_{\bar{r}}^2 - \zeta_{\bar{\theta}}^2), \tag{38b}$$

for $d = 2$. In addition, we introduce the following L^1 norm of $\widetilde{f} - \widetilde{M_w}$ ($d = 1$) in ζ_1, that of $\widetilde{f}^{(2)} - \widetilde{M}_w^{(2)}$ ($d = 2$) in $(\zeta_{\bar{r}},\,\zeta_{\bar{\theta}})$, and that of $f - M_w$ ($d = 3$) in ζ_i, respectively:

$$\|\Delta f\|^{(1)}(|x_1|,\,t) = \int_{-\infty}^{\infty} |\widetilde{f} - \widetilde{M_w}|\mathrm{d}\zeta_1, \tag{39a}$$

$$\|\Delta f\|^{(2)}(\bar{r},\,t) = \int_{-\infty}^{\infty}\int_{-\infty}^{\infty} |\widetilde{f}^{(2)} - \widetilde{M}_w^{(2)}|\mathrm{d}\zeta_{\bar{r}}\mathrm{d}\zeta_{\bar{\theta}}, \tag{39b}$$

$$\|\Delta f\|^{(3)}(r,\,t) = \int_{-\infty}^{\infty}\int_{-\infty}^{\infty}\int_{-\infty}^{\infty} |f - M_w|\mathrm{d}\zeta_r\mathrm{d}\zeta_\theta\mathrm{d}\zeta_\varphi. \tag{39c}$$

We further introduce the average of the above L^1 norms in the vessel, i.e.,

$$\overline{\|\Delta f\|^{(d)}}(t) = 2^d d\int_0^{1/2} \|\Delta f\|^{(d)}\mathrm{d}\mu^{(d)}, \qquad (d = 1,\,2,\,3), \tag{40}$$

where $\mathrm{d}\mu^{(1)} = \mathrm{d}x_1$, $\mathrm{d}\mu^{(2)} = \bar{r}\mathrm{d}\bar{r}$, and $\mathrm{d}\mu^{(3)} = r^2\mathrm{d}r$.

4.2.2 Numerical method

Once $\rho_w(t)$ is known, the macroscopic quantities ρ, u_i, T, and W are obtained by using Eq. (19) in Eqs. (11) and (12). In the present spherically symmetric case, we can calculate the macroscopic quantities at the point $(x_1,\,0,\,0)$ $(0 \leq x_1 \leq 1/2)$. For instance, in the 3D case, $h(r,\,t)$ for $r = x_1$, any θ, and any φ ($h = \rho$, u_r, T, etc., where u_r is the r component of u_i) is given by $h(x_1,\,0,\,0,\,t)$ ($h = \rho$, u_1, T, etc.).

The macroscopic variables at $(x_1,\, 0,\, 0)$ $(0 \le x_1 \le 1/2)$ are expressed as

$$\rho = F_{(0,0,0)} + P_{(0,0,0)}, \quad u_1 = \frac{1}{\rho}\left(F_{(1,0,0)} + P_{(1,0,0)}\right), \tag{41a}$$

$$T = \frac{2}{3\rho}\left(F_{(2,0,0)} + F_{(0,2,0)} + F_{(0,0,2)} + P_{(2,0,0)} + P_{(0,2,0)} + P_{(0,0,2)} - \rho u_1^2\right), \tag{41b}$$

$$W = Q_{(0,0,0)} - \frac{3}{2}\ln T_0\, F_{(0,0,0)} + \left(1 - \frac{1}{T_0}\right)\left(F_{(2,0,0)} + F_{(0,2,0)} + F_{(0,0,2)}\right), \tag{41c}$$

where

$$F_{(n_1,n_2,n_3)} = \int_{\zeta_i \in \Omega_0} \zeta_1^{n_1}\zeta_2^{n_2}\zeta_3^{n_3} f_0(\zeta_i)\mathrm{d}\boldsymbol{\zeta}, \tag{42a}$$

$$P_{(n_1,n_2,n_3)} = \int_{\zeta_i \in \Omega_w} \zeta_1^{n_1}\zeta_2^{n_2}\zeta_3^{n_3} M_w(\zeta_i)\, \rho_w(s)\mathrm{d}\boldsymbol{\zeta}, \tag{42b}$$

$$Q_{(n_1,n_2,n_3)} = \int_{\zeta_i \in \Omega_w} \zeta_1^{n_1}\zeta_2^{n_2}\zeta_3^{n_3} M_w(\zeta_i)\, \rho_w(s)\, \ln \rho_w(s)\, \mathrm{d}\boldsymbol{\zeta}, \tag{42c}$$

Ω_0, Ω_w, and s, which have occurred in Eq. (21), are evaluated at $(x_1,\, 0,\, 0)$, and $u_{\bar{r}}$ (the $\bar{r}$ component of u_i) and u_r at $(x_1,\, 0,\, 0)$ are represented by u_1.

The $F_{(n_1,n_2,n_3)}$ contained in Eq. (41) can be obtained analytically in the form including the error and exponential functions for $d = 1$ and can be reduced to single integrals including the sinusoidal, error, and exponential functions for $d = 2$ and 3. On the other hand, the $P_{(n_1,n_2,n_3)}$ and $Q_{(n_1,n_2,n_3)}$ can be expressed in the form of convolution:

$$P_{(n_1,n_2,n_3)} = \int_0^t K_d(x_1,\, t-s)\rho_w(s)\mathrm{d}s, \tag{43a}$$

$$Q_{(n_1,n_2,n_3)} = \int_0^t K_d(x_1,\, t-s)\rho_w(s)\ln \rho_w(s)\, \mathrm{d}s, \tag{43b}$$

where s is the integration variable. The kernel K_d is expressed analytically in terms of the exponential function for $d = 1$ and is expressed in the form of a single integral of a function containing the sinusoidal and exponential functions for $d = 2$ and 3. The explicit form of $F_{(n_1,n_2,n_3)}$ and K_d are omitted for conciseness.

The single integrals in $F_{(n_1,n_2,n_3)}$ and K_d for $d = 2$ and 3 are evaluated numerically using the Gaussian quadrature, and the accuracy with an error less than 10^{-16} is attained. As for the convolutions (43), we use the values of ρ_w at $t = t_n$ $[\rho_w(t_n) = U_n + 1]$ obtained in Sec. 4.1.2. More specifically, the integral with respect to s is divided into the integrals over small intervals $[s_{m-1},\, s_m]$ $(s_m = m\Delta t)$, in each of which $\rho_w(s)$ is approximated by the linear function, and the integration over each interval is performed numerically using the Gaussian quadrature. The linear approximation of ρ_w is legitimate because the change of $\rho_w(s)$ is moderate and the behavior of the integrands

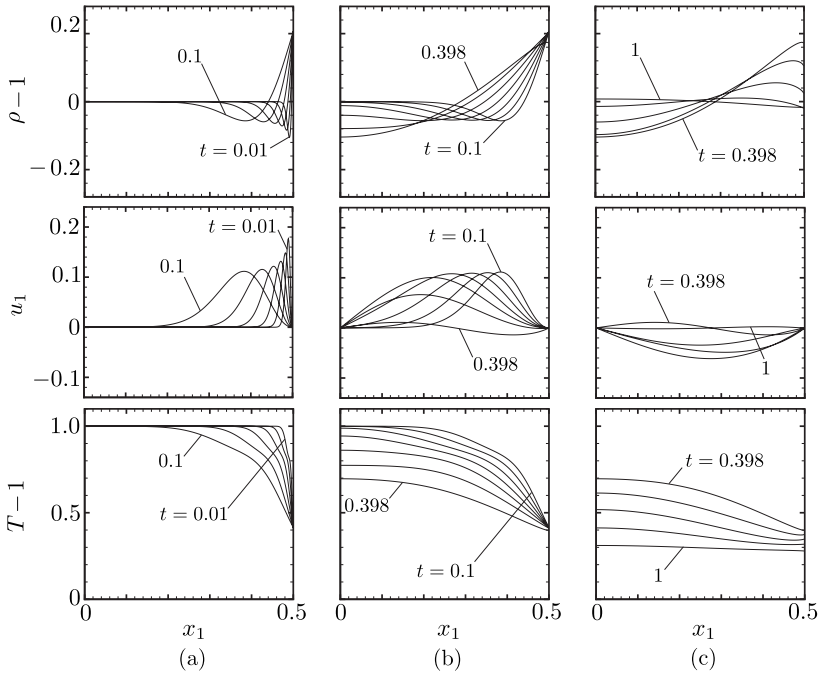

Fig. 3 Short-time behavior of ρ, u_1 and T for $T_0 = 2$ in the 1D case ($d = 1$): ρ, u_1, and T vs x_1 for $0 \le x_1 \le 0.5$. (a) $t = 0.01, 0.0158, 0.0251, 0.0398, 0.0631, 0.1$, (b) $t = 0.1, 0.125, 0.158, 0.199, 0.251, 0.398$, (c) $t = 0.398, 0.501, 0.631, 0.794, 1$.

$K_d(x_1,\, t-s)\rho_w(s)$ and $K_d(x_1,\, t-s)\rho_w(s)\ln\rho_w(s)$ is dominated by that of $K_d(x_1,\, t-s)$. In fact, as the point $(x_1,\, 0,\, 0)$ approaches the vessel wall ($x_1 \approx 1/2$), the change of K_d becomes steeper. In such a case, we ought to decrease the size of the small intervals $[s_{m-1},\, s_m]$, i.e., the time step Δt. That is, the smallness of the time step Δt in solving Eq. (32) is determined not only by the behavior of the solution itself but also by the requirement that the integrals (43) be obtained accurately even near the vessel wall. Incidentally, the values of the macroscopic quantities at the vessel wall ($x_1 = 1/2$) are obtained differently.

The computation of the L^1 norms (39) is similar to that of ρ. In fact, we can show that there is a time t_c (depending on d and T_0) such that, for $t > t_c$, the $f - M_w$, $\widetilde{f} - \widetilde{M}_w$, or $\widetilde{f}^{(2)} - \widetilde{M}_w^{(2)}$ in Eq. (39) does not change sign. Therefore, if we restrict ourselves to the long-time behavior, the computation is essentially the same as that for ρ.

5 Results of numerical analysis

In this section, we summarize the results obtained by numerical analysis. Here, it should be recalled that the numerical computation is based on the

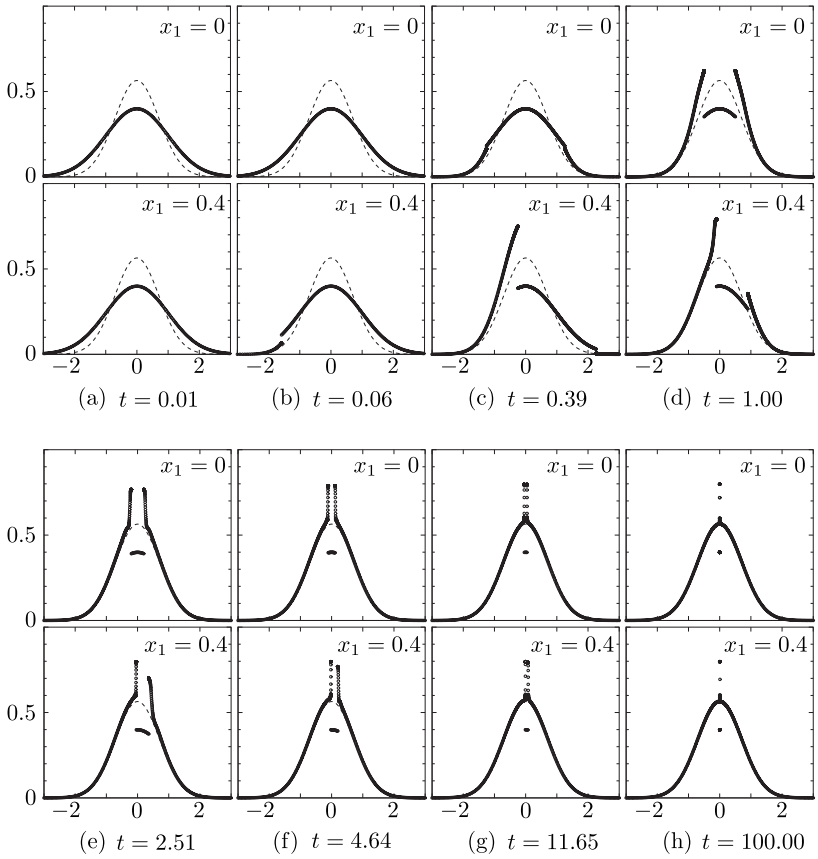

Fig. 4 Time evolution of the marginal velocity distribution function $\widetilde{f}(x_1, \zeta_1, t)$ for $T_0 = 2$ in the 1D case ($d = 1$). $\widetilde{f}$ vs ζ_1 is shown at different times. (a) $t = 0.01$, (b) $t = 0.06$, (c) $t = 0.39$, (d) $t = 1.00$, (e) $t = 2.51$, (f) $t = 4.64$, (g) $t = 11.65$, (h) $t = 100.00$. Here, the upper figures show the results at $x_1 = 0$, and the lower at $x_1 = 0.4$; the dashed line indicates $\widetilde{M}_w$.

initial condition (23). If a more general initial condition with the concentration of mass at $\zeta_i = 0$ is considered (e.g., a class of functions with $\langle W(f_0|M_w)\rangle$ being finite), the resulting decay rate, Eqs. (46), (48), and (49), may change.

5.1 Short- and intermediate-time behavior

First, we show some results for relatively short times. Figure 3 shows the time evolution of the profiles of the density, flow velocity, and temperature for $T_0 = 2$ in the 1D case ($d = 1$): Figs. 3(a), 3(b), and 3(c) are, respectively, for $0.01 \le t \le 0.1$, $0.1 \le t \le 0.398$, and $0.398 \le t \le 1$. Disturbances are created at the boundary and propagate in the interior domain. At $t = 1$, ρ

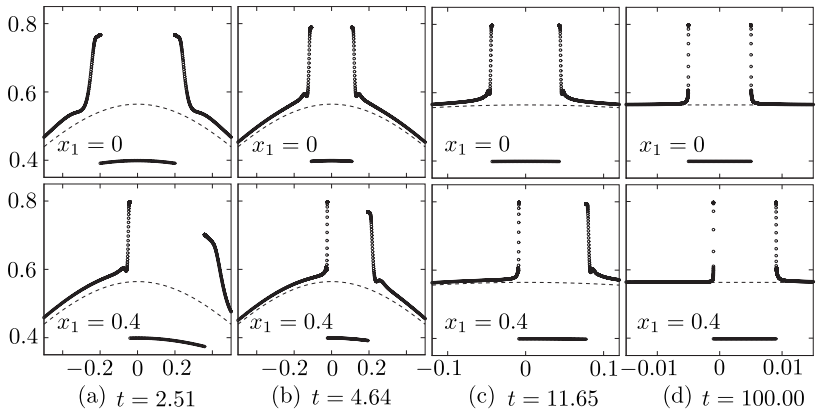

Fig. 5 Time evolution of the marginal velocity distribution function $\widetilde{f}(x_1, \zeta_1, t)$ for $T_0 = 2$ in the 1D case ($d = 1$). (a) $t = 2.51$, (b) $t = 4.64$, (c) $t = 11.65$, (d) $t = 100.00$. Figures (a), (b), (c) and (d) are enlarged versions of Fig. 4 (e), (f), (g) and (h), respectively. See the caption of Fig. 4.

and u_1 are already close to their final values ($\rho = 1$ and $u_1 = 0$), whereas T is still far from it ($T = 1$) though T is almost uniform. In the 2D and 3D cases, the results for which are omitted here, the disturbances are larger, but decay faster.

Figures 4 and 5 show the time evolution of the marginal velocity distribution function $\widetilde{f}$ defined by Eq. (37a) for the 1D case as the function of ζ_1 at the center of the gap $x_1 = 0$ and at $x_1 = 0.4$; the upper figures show $\widetilde{f}$ at $x_1 = 0$, and the lower at $x_1 = 0.4$; Figs. 5(a)–(d) are enlarged versions of Figs. 4(e)–(h) near $\zeta_1 = 0$; the dashed line indicates the marginal $\widetilde{M}_w$ corresponding to the final steady state M_w [Eq. (37b)].

In the 1D case with the initial condition (23), the marginal $\widetilde{f}$ is expressed as [cf. Eq. (19)]

$$\widetilde{f}(x_1, \zeta_1, t) = \begin{cases} \dfrac{1}{\sqrt{\pi T_0}} \exp\Big(- \dfrac{\zeta_1^2}{T_0}\Big), & \Big(\dfrac{x_1 - 1/2}{t} < \zeta_1 < \dfrac{x_1 + 1/2}{t}\Big), \\ \dfrac{1}{\sqrt{\pi}} \rho_w\Big(t - \dfrac{x_1 - 1/2}{\zeta_1}\Big) \exp(-\zeta_1^2), & \Big(\zeta_1 < \dfrac{x_1 - 1/2}{t}\Big), \\ \dfrac{1}{\sqrt{\pi}} \rho_w\Big(t - \dfrac{x_1 + 1/2}{\zeta_1}\Big) \exp(-\zeta_1^2), & \Big(\dfrac{x_1 + 1/2}{t} < \zeta_1\Big). \end{cases} \tag{44}$$

Let us consider the evolution of $\widetilde{f}$ at $x_1 = 0$ (upper figures of Figs. 4 and 5), referring to Eq. (44). The molecules in the range $-1/2t < \zeta_1 < 1/2t$, which shrinks as time goes on, come directly from the initial distribution without interaction with the walls (see Figs. 4 and 5). At the initial stages, the molecules distributed according to the initial distribution impinge on the walls and are reflected. Since $T_0 > 1$ in Figs. 4 and 5, the reflected molecules are cooled down. In other words, less fast molecules (the molecules

with large $|\zeta_1|$) and more slow molecules (the molecules with small $|\zeta_1|$) are produced by the reflection. At an early time [Fig. 4(c)], only the less-crowded fast molecules among the reflected molecules can reach the point $x_1 = 0$. Therefore, the high-speed tail of the distribution is reduced compared with the initial distribution. At a later time [Fig. 4(d)], the more-crowded slow molecules with speed $|\zeta_1| \approx 1/2t$ ($1/2t < |\zeta_1| < 1/2t + \delta$ with δ a small number) reflected at the initial stages reach the point $x_1 = 0$. This results in a significant increase of $\widetilde{f}$ for this speed range. At large times [Figs. 4(e)–(h) and Figs. 5(a)–(d)], the range of the more-crowded slow molecules with speed $|\zeta_1| \approx 1/2t$ reflected at the initial stages is more and more localized because slightly faster molecules have already experienced many reflections, so that they are well accommodated with the walls (or they are close to the final equilibrium state). At point $x_1 = 0.4$, which is closer to the right wall ($x_1 = 1/2$), the increase of $\widetilde{f}$ for negative ζ_1 is observed much earlier [Fig. 4(c)] than at $x_1 = 0$, since the more-crowded slow molecules reflected on the right wall at the initial stages reach the point ($x_1 = 0.4$) much earlier than the corresponding molecules from the left wall ($x_1 = -1/2$). However, except for the non-symmetry, the manner of deformation of $\widetilde{f}$ is essentially the same.

The localized deviation in $\widetilde{f}$ in the neighborhood of $\zeta_1 = (x_1 \pm 1/2)/t$ exists forever though the range shrinks as time goes on. This is a sort of long-memory effect originating from the very initial stages, which leads to the slow decay of the velocity-averaged quantities, as we will see in Sec. 5.2.

A mathematical description (estimate) corresponding to the deformation of the velocity distribution function explained in the preceding paragraphs is given in [15]. The effect of the slow molecules (or molecules moving parallel to the boundary) also manifests itself in the diffusion limit where the thickness of the channel containing a free-molecular gas is led to zero [20–22]. It should also be mentioned that a different type of long-memory effect, arising in the unsteady motion of a body in a free-molecular gas, has been investigated in [23–26].

5.2 Long-time behavior and approach to equilibrium

Next, we investigate the long-time behavior and the approach to the final equilibrium state, which is the main purpose of the present study. In what follows, the logarithm $\log(\cdot)$ indicates the common logarithm with base 10.

5.2.1 $\rho_w(t)$

The crucial quantity is $\rho_w(t)$, from which the velocity distribution function and thus all the macroscopic quantities can be obtained. The long-time behavior of ρ_w is shown in Fig. 6 and Table 1 for the 1D, 2D, and 3D cases. Figure 6(a) shows $\log|\rho_w - 1|$ versus $\log t$ for $T_0 = 2$, and Fig. 6(b) the gradients of the curves in Fig. 6(a) versus $\log t$. Here, $\alpha(h)$ for a function $h(t)$ is defined by

$$\alpha(h) = \mathrm{d}\log|h(t) - h_\infty|/\mathrm{d}\log t, \tag{45}$$

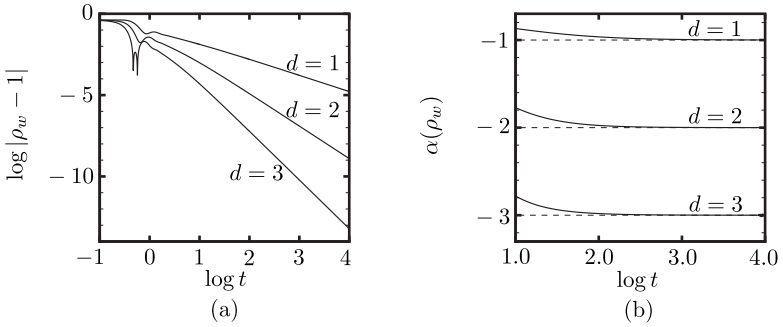

Fig. 6 Long-time behavior of ρ_w for different dimension $d = 1$, 2, and 3 for $T_0 = 2$. (a) $\log|\rho_w - 1|$ vs $\log t$, (b) $\alpha(\rho_w)$ vs $\log t$.

Table 1 Values of $\alpha(\rho_w)$ at large times for different T_0.

		$-\alpha(\rho_w)$ $(d = 1)$			
t	$\log t$	$T_0 = 0.5$	$T_0 = 0.8$	$T_0 = 1.5$	$T_0 = 2.0$
316	2.5	0.984778	0.984559	0.984292	0.984178
1000	3.0	0.993830	0.993760	0.993673	0.993637
3162	3.5	0.997626	0.997604	0.997576	0.997565
10000	4.0	0.999117	0.999110	0.999101	0.999098
		$-\alpha(\rho_w)$ $(d = 2)$			
t	$\log t$	$T_0 = 0.5$	$T_0 = 0.8$	$T_0 = 1.5$	$T_0 = 2.0$
316	2.5	1.993056	1.992784	1.992415	1.992248
1000	3.0	1.997843	1.997756	1.997638	1.997585
3162	3.5	1.999323	1.999295	1.999258	1.999241
10000	4.0	⋯	⋯	⋯	1.999760
		$-\alpha(\rho_w)$ $(d = 3)$			
t	$\log t$	$T_0 = 0.5$	$T_0 = 0.8$	$T_0 = 1.5$	$T_0 = 2.0$
316	2.5	2.995022	2.994742	2.994320	2.994118
1000	3.0	2.998437	2.998348	2.998214	2.998150
3162	3.5	⋯	⋯	⋯	2.999415
5011	3.7	⋯	⋯	⋯	2.999626

where h_∞ indicates the equilibrium value of $h(t)$, e.g., $\rho_{w\infty} = 1$. Table 1 contains the values of $\alpha(\rho_w)$ at large times for different T_0. From these results, it is highly probable that $\rho_w - 1$ decays as

$$|\rho_w - 1| \approx C_w^{(d)}/t^d, \qquad (d = 1,\ 2,\ 3), \tag{46}$$

with positive constants $C_w^{(d)}$.

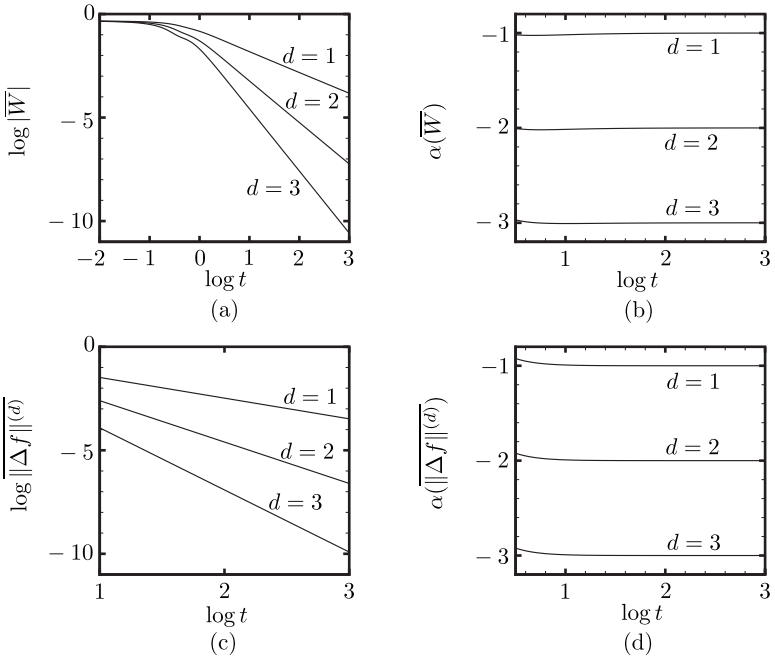

Fig. 7 Long-time behavior of $\overline{W}$ and $\overline{\|\Delta f\|^{(d)}}$ for different dimension $d = 1$, 2, and 3 for $T_0 = 2$. (a) $\log|\overline{W}|$ vs $\log t$, (b) $\alpha(\overline{W})$ vs $\log t$, (c) $\log\overline{\|\Delta f\|^{(d)}}$ vs $\log t$, (d) $\alpha(\overline{\|\Delta f\|^{(d)}})$ vs $\log t$.

5.2.2 Global quantities

Next, we show the long time behavior of the global quantities, $\overline{\|\Delta f\|^{(d)}}(t)$ [Eq. (40)] and $\overline{W}(t)$, where $\overline{W}(t)$ is defined by Eq. (40) with $\|\Delta f\|^{(d)}$ replaced by W [Eq. (12)] [note that $W = W(|x_1|, t)$ for $d = 1$, $W = W(\bar{r}, t)$ for $d = 2$, and $W = W(r, t)$ for $d = 3$ in the present case]. It should be noted that

$$\overline{W} = \langle W\rangle/\mathrm{vol}(\mathcal{D}), \tag{47}$$

where $\langle W\rangle$ is defined in Eq. (16), $\mathrm{vol}(\mathcal{D})$ is the volume of the vessel (with the obvious interpretation in the 1D and 2D cases) in the dimensionless x_i space. Figure 7(a) shows $\log|\overline{W}|$ versus $\log t$ for $-2 \le \log t \le 3$, and Fig. 7(b) the gradients $\alpha(\overline{W})$ [cf. Eq. (45)] of the curves in Fig. 7(a) versus $\log t$; Fig. 7(c) shows $\log\overline{\|\Delta f\|^{(d)}}$ versus $\log t$ for $1 \le \log t \le 3$, and Fig. 7(d) the gradients $\alpha(\overline{\|\Delta f\|^{(d)}})$ of the curves in Fig. 7(c) versus $\log t$. Table 2 shows the values of the gradients $\alpha(\overline{W})$ and $\alpha(\overline{\|\Delta f\|^{(d)}})$ at $t = 10000$ for $T_0 = 0.5$, 0.8, 1.5, and 2 in the 1D case and those at $t = 1000$ for $T_0 = 2$ in the 2D and 3D cases. As mentioned in the last paragraph in Sec. 2.2, $\langle W\rangle$ and thus $\overline{W}$ decrease monotonically. In order to demonstrate this property, the curves in Fig. 7(a) are plotted from a very short time ($t = 0.01$). Figure 7 and Table 2 provide

Table 2 Values of $\alpha(\overline{W})$ and $\alpha(\overline{\|\Delta f\|^{(d)}})$ at $t = 10000$ for $d = 1$ and $t = 1000$ for $d = 2$ and 3.

			$-\alpha(\overline{W})$			
d	t	$\log t$	$T_0 = 0.5$	$T_0 = 0.8$	$T_0 = 1.5$	$T_0 = 2.0$
1	10^4	4	1.000028	1.000027	1.000025	1.000025
2	10^3	3	$\cdots$	$\cdots$	$\cdots$	2.000194
3	10^3	3	$\cdots$	$\cdots$	$\cdots$	3.000163
			$-\alpha(\overline{\|\Delta f\|^{(d)}})$			
d	t	$\log t$	$T_0 = 0.5$	$T_0 = 0.8$	$T_0 = 1.5$	$T_0 = 2.0$
1	10^4	4	0.999999	0.999999	0.999999	0.999999
2	10^3	3	$\cdots$	$\cdots$	$\cdots$	1.999997
3	10^3	3	$\cdots$	$\cdots$	$\cdots$	2.999998

numerical evidence that $\overline{W}$ and $\overline{\|\Delta f\|^{(d)}}$ decay as

$$|\overline{W}| \approx \overline{C}_W^{(d)}/t^d, \qquad \overline{\|\Delta f\|^{(d)}} \approx \overline{C}_\Delta^{(d)}/t^d, \qquad (d = 1,\, 2,\, 3), \tag{48}$$

where $\overline{C}_W^{(d)}$ and $\overline{C}_\Delta^{(d)}$ are positive constants, that is, evidence that Eq. (2) is true.

5.2.3 Local macroscopic quantities

Finally, we show the long-time behavior of the local macroscopic quantities. Figure 8(a) shows $\log|W|$ versus $\log t$, Fig. 8(b) the gradients $\alpha(W)$ [cf. Eq. (45)] of the curves in Fig. 8(a) versus $\log t$, Fig. 8(c) $\log\|\Delta f\|^{(1)}$ versus $\log t$, and Fig. 8(d) the gradients $\alpha(\|\Delta f\|^{(1)})$ [cf. Eq. (45)] of the curves in Fig. 8(c) versus $\log t$, at several x_1 for $T_0 = 2$ in the 1D case ($d = 1$). In Fig. 9, we show the behavior of the density ρ, flow velocity u_1, and temperature T at some points for $T_0 = 2$ in the 1D case ($d = 1$); Fig. 9(a) is the plot of $\log|h - h_\infty|$ versus $\log t$, where $h = \rho$, u_1, and T ($\rho_\infty = T_\infty = 1$, $u_{1\infty} = 0$), and Figs. 9(b), 9(c), and 9(d) show the gradients of the curves in 9(a) for ρ, u_1, and T, respectively. Figures 10(a), 10(b), and 10(c) are the figures in the 2D case ($d = 2$) and Figs. 11(a), 11(b), and 11(c) those in the 3D case ($d = 3$) corresponding to Figs. 8(a), 8(c), and 9(a) [the curves at less points are shown in Figs. 10(a), 10(b), 11(a), and 11(b)]. The curves for the evolution of the gradients corresponding to Figs. 8(b), 8(d), 9(b), 9(c), and 9(d) are omitted for the 2D and 3D cases. Table 3 contains the values of the gradients $\alpha(h)$ with $h = W$, $\|\Delta f\|^{(d)}$, ρ, u_1 ($d = 1$), $u_{\bar{r}}$ ($d = 2$), u_r ($d = 3$), and T at a point ($x_1 = 0.2$ for $d = 1$, $\bar{r} = 0.2$ for $d = 2$, and $r = 0.2$ for $d = 3$) for various T_0 at a long time ($t = 10000$ for $d = 1$, $t = 3162$ for $d = 2$, and $t = 1000$ for $d = 3$). From these results, we observe that $\alpha(W)$, $\alpha(\|\Delta f\|^{(d)})$, and $\alpha(T)$ tend to approach $-d$, whereas $\alpha(\rho)$ tends to approach $-(d+1)$. In addition, $\alpha(u_1)$, $\alpha(u_{\bar{r}})$, and $\alpha(u_r)$ tend to approach -3, -4, and

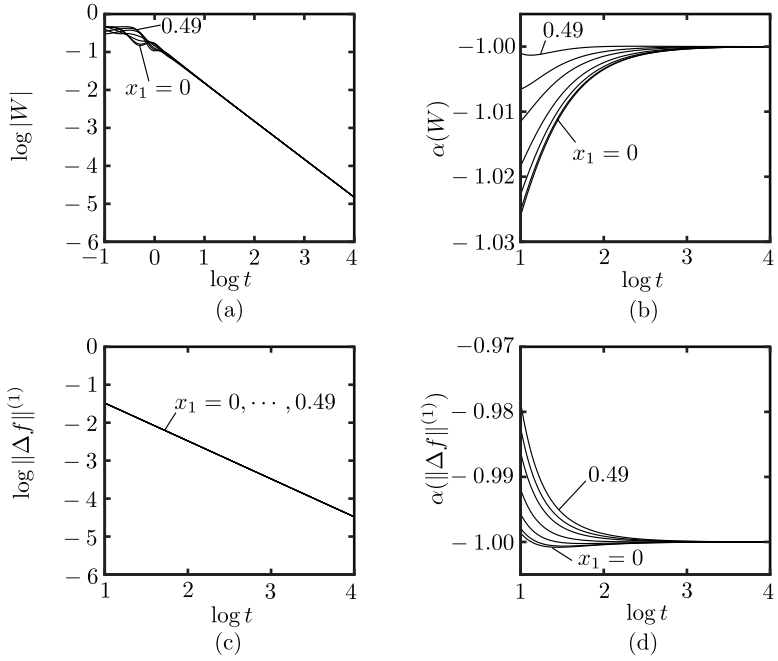

Fig. 8 Long-time behavior of W and $\|\Delta f\|^{(1)}$ at $x_1 = 0$, 0.1, 0.2, 0.3, 0.4, 0.45, 0.49 for $T_0 = 2$ ($d = 1$). (a) $\log|W|$ vs $\log t$, (b) $\alpha(W)$ vs $\log t$, (c) $\log\|\Delta f\|^{(d)}$ vs $\log t$, (d) $\alpha(\|\Delta f\|^{(1)})$ vs $\log t$.

-5, respectively. This gives numerical evidence of the following decay rates:

$$\begin{aligned} &|W| \approx C_W^{(d)}/t^d, \quad \|\Delta f\|^{(d)} \approx C_\Delta^{(d)}/t^d, \\ &|T-1| \approx C_T^{(d)}/t^d, \quad |\rho - 1| \approx C_\rho^{(d)}/t^{d+1}, \\ &|u_1| \approx C_1^{(1)}/t^3, \quad |u_{\bar{r}}| \approx C_{\bar{r}}^{(2)}/t^4, \quad |u_r| \approx C_r^{(3)}/t^5, \end{aligned} \tag{49}$$

where $C_W^{(d)}$, $C_\Delta^{(d)}$, etc. are positive constants, depending on the position in space. As we can see from Figs. 8–11, it is likely that $C_W^{(d)}$, $C_\Delta^{(d)}$, and $C_T^{(d)}$ are independent of position. It should be noted that the density and flow velocity decay faster than the temperature, relative entropy (W), and L^1 norm ($\|\Delta f\|^{(d)}$).

5.2.4 Remarks on accuracy of computation

The accuracy of the numerical solution of Eq. (32) depends on the quadrature for numerical integration (33) and the time step Δt. The results in Table 1 are obtained with $\Delta t = 0.002$. In the case of $T_0 = 2$, we have also carried out the computation with different time steps, $\Delta t = 0.01$, 0.005, and 0.001, until $\log t = 4$ ($d = 1$) and 3 ($d = 2,\ 3$). The results for $\alpha(\rho_w)$ based on

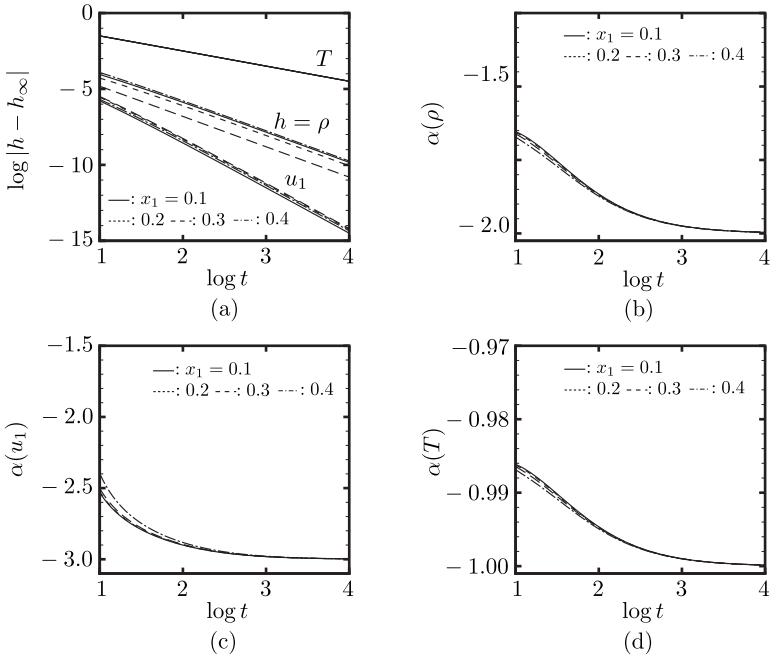

Fig. 9 Long-time behavior of ρ, u_1 and T at $x_1 = 0.1$, 0.2, 0.3, 0.4 for $T_0 = 2$ ($d = 1$). (a) $\log|h - h_\infty|$ vs $\log t$, where $h = \rho$, u_1 and T, (b) $\alpha(\rho)$ vs $\log t$, (c) $\alpha(u_1)$ vs $\log t$, (d) $\alpha(T)$ vs $\log t$. Here, the solid line indicates the quantities at $x_1 = 0.1$, the dashed line at $x_1 = 0.2$, the long-dashed line at $x_1 = 0.3$, and the dot-dashed line at $x_1 = 0.4$.

different time steps agree until the seventh decimal place. Therefore, it is highly probable that all the values in Table 1 are accurate until the last decimal place. In the 3D case, the decay of $|\rho_w - 1|$ is faster, and it becomes less than 10^{-13} at $\log t = 4$. Therefore, it becomes very difficult to obtain the gradient of the curve accurately by the method described in the last paragraph in this subsection. In fact, the curve for $d = 3$ in Fig. 6(b) exhibits small oscillation for $\log t$ close to 4. This is the reason why $\alpha(\rho_w)$ for $d = 3$ and $T_0 = 2$ is shown only up to $\log t = 3.7$ in Table 1.

As explained in the second from last paragraph in Sec. 4.2.2, if we want to obtain the macroscopic quantities accurately near the vessel wall, we need a time step smaller than required by Eq. (32) itself. The time step $\Delta t = 0.002$, which might appear unnecessarily small, is chosen in such a way that the macroscopic variables at (0.49, 0, 0) are obtained accurately.

The results in Table 3 are also based on $\Delta t = 0.002$. At $\log t = 3$ and at $x_1 = 0$, 0.2, and 0.4 ($x_2 = x_3 = 0$), the gradients $\alpha(W)$, $\alpha(\|\Delta f\|^{(d)})$, and $\alpha(T)$ with $\Delta t = 0.002$ agree with those with $\Delta t = 0.001$ up to the fifth decimal place for $d = 1$, 2, and 3. But, the agreement is one or two fewer decimal places for $\alpha(\rho)$ and $\alpha(u)$ ($u = u_1$, $u_{\bar{r}}$, or u_r).

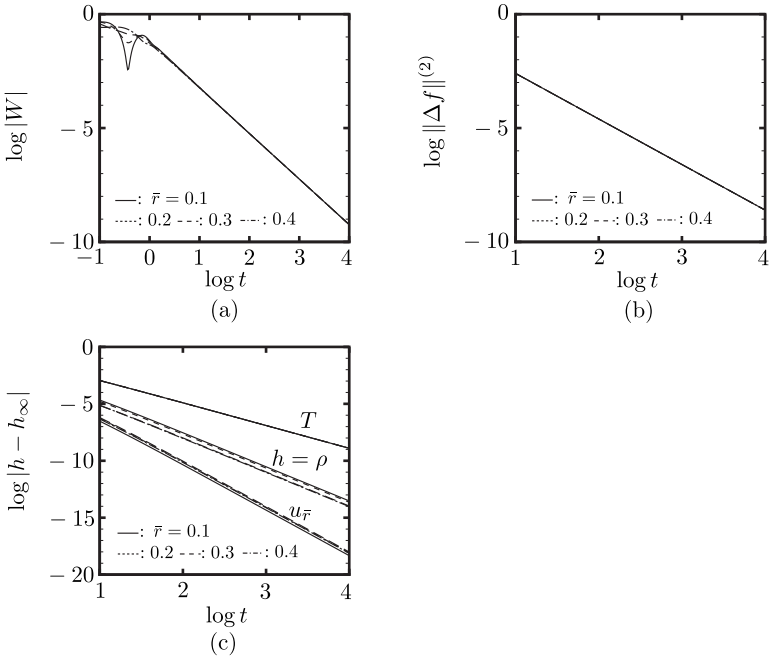

Fig. 10 Long-time behavior of W, $\|\Delta f\|^{(2)}$, ρ, $u_{\bar{r}}$, and T at $\bar{r} = 0.1$, 0.2, 0.3, 0.4 for $T_0 = 2$ ($d = 2$). (a) $\log|W|$ vs $\log t$. (b) $\log\|\Delta f\|^{(2)}$ vs $\log t$. (c) $\log|h - h_\infty|$ vs $\log t$, where $h = \rho$, $u_{\bar{r}}$, and T. Here, the solid line indicates the quantities at $\bar{r} = 0.1$, the dashed line at $\bar{r} = 0.2$, the long-dashed line at $\bar{r} = 0.3$, and the dot-dashed line at $\bar{r} = 0.4$.

The values of $\alpha(\overline{W})$ and $\alpha(\overline{\|\Delta f\|^{(d)}})$ in Table 2 are also based on the data obtained with $\Delta t = 0.002$. Here, the integration with respect to the space variable [cf. (40)] is carried out analytically for $d = 1$ and numerically for $d = 2$ and 3. In the latter, Simpson's rule with a uniform interval Δx ($x = \bar{r}$ or r) is used. The data for $d = 2$ and 3 in Table 2 are obtained with $\Delta x = 0.005$. However, the results obtained with $\Delta x = 0.025$ and 0.01 do not show any difference from the values in Table 2.

The gradient $\alpha(\rho_w)$ [cf. Eq. (45)] shown in Fig. 6(b) and Table 1 is evaluated by simple linear approximation, i.e., $\alpha(\rho_w)(t_n) = (\log|U_n| - \log|U_{n-1}|)/(\log t_n - \log t_{n-1})$. On the other hand, once $\rho_w(t)$ is obtained, we can obtain the macroscopic quantities at any point in space and at any t. We evaluate the macroscopic quantities at discrete t's, say $t = \bar{t}_m$, which are distributed uniformly in $\log t$ (50 points in the interval $n < \log t \le n + 1$ with n being integer). Then, the gradient $\alpha(h)$ is obtained by simple linear approximation.

The computation was carried out with quadruple precision. If we perform the computation with double precision, we are not able to show the convergence of the gradients $\alpha(\rho_w)$, $\alpha(W)$, $\alpha(\rho)$, etc. It should be mentioned that we have employed fast algorithms for the error and Bessel functions provided by T. Ooura, available from his home page (http://www.kurims.kyoto-

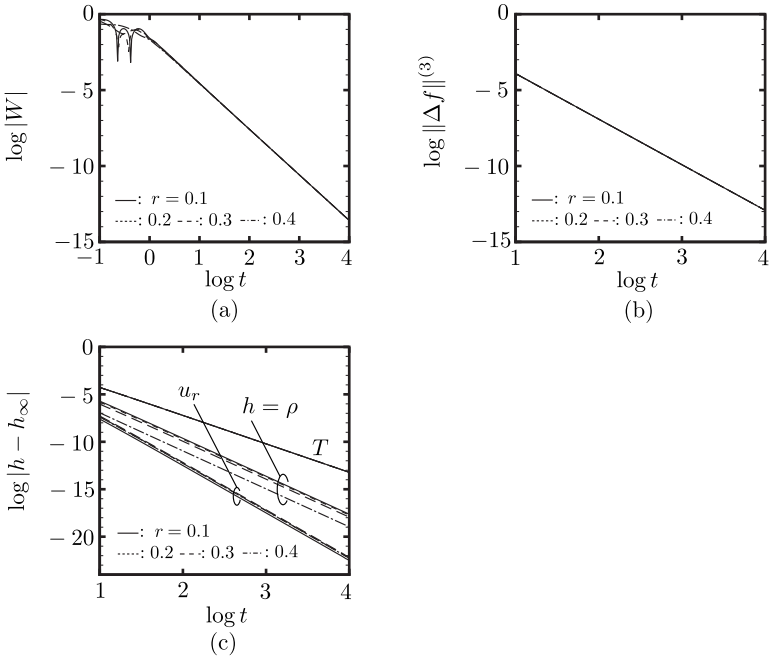

Fig. 11 Long-time behavior of W, $\|\Delta f\|^{(3)}$, ρ, u_r, and T at $r = 0.1$, 0.2, 0.3, 0.4 for $T_0 = 2$ ($d = 3$). (a) $\log|W|$ vs $\log t$. (b) $\log\|\Delta f\|^{(3)}$ vs $\log t$. (c) $\log|h - h_\infty|$ vs $\log t$, where $h = \rho$, u_r, and T. Here, the solid line indicates the quantities at $r = 0.1$, the dashed line at $r = 0.2$, the long-dashed line at $r = 0.3$, and the dot-dashed line at $r = 0.4$.

u.ac.jp/˜ooura/index.html). The algorithms are for double precision, but we have confirmed that they give an accuracy of 19 significant figures if they are used in a quadruple-precision computation.

The computation has been carried out on a PC cluster with CPU: Intel(R) Core 2 Extreme QX9650 3.0GHz(4CPU)×8.

6 Non-symmetric initial condition (one-dimensional case)

In Secs. 4 and 5, we investigated the time evolution of the solution with initial condition (23), i.e., a uniform equilibrium state at rest with a temperature different from the temperature of the vessel wall. In this section, restricting ourselves to the 1D case, we repeat the same computation with a non-symmetric initial condition. Our initial condition is

$$f_0(x_1, \zeta_i) = \frac{\rho^{\mathrm{in}}(x_1)}{[\pi T^{\mathrm{in}}(x_1)]^{3/2}} \exp\Big(- \frac{[\zeta_1 - u_1^{\mathrm{in}}(x_1)]^2 + \zeta_2^2 + \zeta_3^2}{T^{\mathrm{in}}(x_1)}\Big), \tag{50}$$

Table 3 Values of $\alpha(h)$ at large t for different T_0 ($d = 1$, 2, 3).

	$-\alpha(h)$ $(d = 1,\ x_1 = 0.2,\ t = 10000)$			
h	$T_0 = 0.5$	$T_0 = 0.8$	$T_0 = 1.5$	$T_0 = 2.0$
W	1.000040	1.000064	1.000006	1.000014
$\|\Delta f\|^{(1)}$	0.999994	0.999994	0.999994	0.999994
ρ	1.998055	1.997862	1.998454	1.998414
u_1	2.997527	2.998085	2.996390	2.996803
T	0.999811	0.999824	0.999844	0.999854
	$-\alpha(h)$ $(d = 2,\ \bar{r} = 0.2,\ t = 3162)$			
h	$T_0 = 0.5$	$T_0 = 0.8$	$T_0 = 1.5$	$T_0 = 2.0$
W	1.999919	1.999677	2.000857	2.000198
$\|\Delta f\|^{(2)}$	2.000031	2.000031	2.000030	2.000030
ρ	2.998974	2.999090	2.998970	2.998987
$u_{\bar{r}}$	3.998626	3.998776	3.998653	3.998672
T	1.999657	1.999657	1.999638	1.999626
	$-\alpha(h)$ $(d = 3,\ r = 0.2,\ t = 1000)$			
h	$T_0 = 0.5$	$T_0 = 0.8$	$T_0 = 1.5$	$T_0 = 2.0$
W	2.999493	2.998174	3.001350	3.000942
$\|\Delta f\|^{(3)}$	3.000166	3.000166	3.000166	3.000167
ρ	3.998371	3.998527	3.998369	3.998338
u_r	4.997977	4.998174	4.998001	4.997962
T	2.999152	2.999049	2.998942	2.998874

where

$$\rho^{\rm in}(x_1) = 1 + a_\rho \cos(2\pi m_\rho x_1 + b_\rho), \tag{51a}$$

$$u_1^{\rm in}(x_1) = a_u \cos(2\pi m_u x_1 + b_u), \tag{51b}$$

$$T^{\rm in}(x_1) = 1 + a_T \cos(2\pi m_T x_1 + b_T). \tag{51c}$$

Equation (50) is the local Maxwellian distribution with density $\rho^{\rm in}(x_1)\rho_{0*}$, flow velocity $(u_1^{\rm in}(x_1)c_{w*},\ 0,\ 0)$, and temperature $T^{\rm in}(x_1)T_{w*}$. It should be noted that Eq. (50) with Eq. (51) is a mild function without the concentration of mass at $\zeta_i = 0$. In the present case, Eq. (21) yields a coupled integral equation of renewal type for $\rho_{w-}(t) \equiv \rho_w(\text{at}\quad x_1 = -1/2)$ and $\rho_{w+}(t) \equiv \rho_w(\text{at}\quad x_1 = 1/2)$ in place of Eq. (25) with Eq. (26). We have carried out computations for different values of the parameters a_ρ, m_ρ, etc. Here, we give only the result for the long-time behavior of one case: $(a_\rho,\ b_\rho,\ m_\rho) = (0.5,\ 1,\ 1)$, $(a_u,\ b_u,\ m_u) = (0.5,\ 1,\ 1)$, $(a_T,\ b_T,\ m_T) = (0.5,\ 2,\ 1.5)$.

We show the long-time behavior of $\rho_{w\pm}(t)$ in Fig. 12: Fig. 12(a) shows $\log|\rho_{w\pm} - 1|$ versus $\log t$, and Fig. 12(b) the gradients $\alpha(\rho_{w\pm})$ [cf. Eq. (45)] versus $\log t$. The values of the gradients $\alpha(\rho_{w\pm})$ at some large times are shown in Table 4. It is seen from these results that $\rho_{w\pm}(t) - 1$ tend to decay as

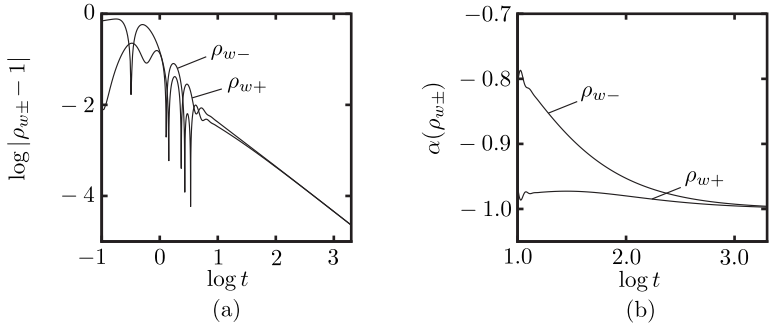

Fig. 12 Long-time behavior of $\rho_{w-}(t)$ and $\rho_{w+}(t)$ for the non-symmetric initial condition ($d = 1$). (a) $\log|\rho_{w\pm} - 1|$ vs $\log t$. (b) $\alpha(\rho_{w\pm})$ vs $\log t$.

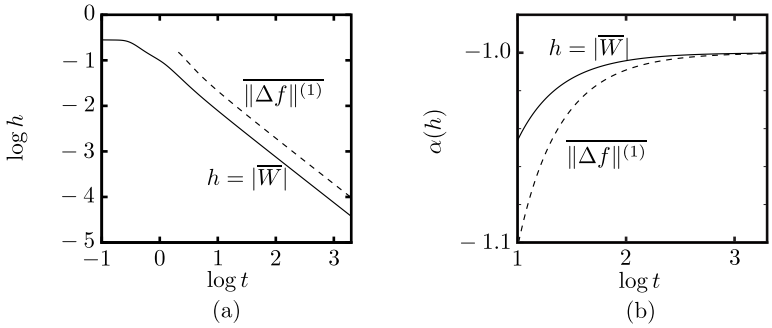

Fig. 13 Long-time behavior of $\overline{W}$ and $\overline{\|\Delta f\|^{(1)}}$ for the non-symmetric initial condition ($d = 1$). (a) $\log|\overline{W}|$ and $\log\overline{\|\Delta f\|^{(1)}}$ vs $\log t$. (b) $\alpha(\overline{W})$ and $\alpha(\overline{\|\Delta f\|^{(1)}})$ vs $\log t$. Here, solid line indicates the quantities of $\overline{W}$, and the dashed line those of $\overline{\|\Delta f\|^{(1)}}$.

Eq. (46) with $d = 1$. Figure 13(a) shows the plots of $\log|\overline{W}|$ and $\log\overline{\|\Delta f\|^{(1)}}$ versus $\log t$, and Fig. 13(b) the gradients $\alpha(\overline{W})$ and $\alpha(\overline{\|\Delta f\|^{(1)}})$ versus $\log t$. Figures 14(a), 14(b), and 14(c) are the figures corresponding to Figs. 8(a), 8(c), and 9(a) [the curves at less points are shown in Figs. 14(a) and 14(b)]. The curves for the evolution of the gradients corresponding to Figs. 8(b), 8(d), 9(b), 9(c), and 9(d) are omitted in the present case. Table 5 shows the values of the gradients $\alpha(h)$ with $h = W$, $\|\Delta f\|^{(1)}$, ρ, u_1, and T at a point ($x_1 = 0.2$) at a long time ($t = 2000$). It is seen from these results that the manner of approach to the final equilibrium state expressed by Eqs. (48) and (49) is also true in the present case.

It should be noted that, with the non-symmetric initial condition (50), the computation becomes more difficult than that in Secs. 4 and 5 to obtain an accurate solution [even with Eq. (50), if $\rho^{\rm in}(x_1)$, $u_1^{\rm in}(x_1)$, and $T^{\rm in}(x_1)$ are chosen in such a way that $\rho_{w-}(0) = \rho_{w+}(0)$ holds at $t = 0$, it becomes easier to get an

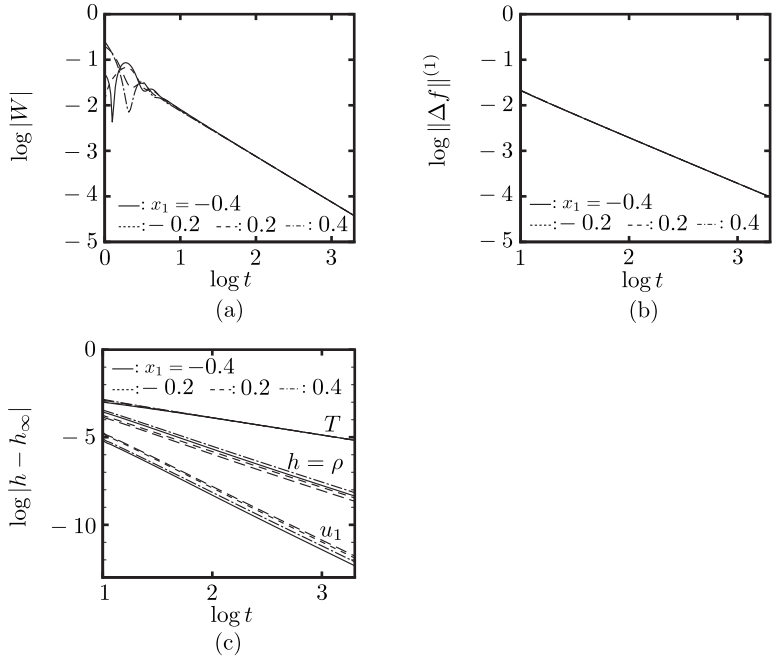

Fig. 14 Long-time behavior of macroscopic quantities W, $\|\Delta f\|^{(1)}$, ρ, u_1 and T at $x_1 = -0.4$, -0.2, 0.2, and 0.4 for the non-symmetric initial condition ($d = 1$). (a) $\log|W|$ vs $\log t$. (b) $\log\|\Delta f\|^{(1)}$ vs $\log t$. (c) $\log|h - h_\infty|$ vs $\log t$, where $h = \rho$, u_1 and T. Here, the solid line indicates the quantities at $x_1 = -0.4$, the dashed line at $x_1 = -0.2$, the long-dashed line at $x_1 = 0.2$, and the dot-dashed line at $x_1 = 0.4$.

Table 4 Values of $\alpha(\rho_{w\pm})$ at large t for the non-symmetric initial condition ($d = 1$).

t	$\log t$	$-\alpha(\rho_{w-})$	$-\alpha(\rho_{w+})$
50	1.698	0.921745	0.974493
100	2.000	0.952926	0.979931
500	2.698	0.986831	0.992228
1000	3.000	0.992608	0.995298
2000	3.301	0.995904	0.997245

accurate result]. Therefore, a smaller time step and a more accurate interpolation formula have been used to obtain the results shown in this section. For instance, $\Delta t = 0.001$ is used, and the quartic approximation, rather than the linear approximation, is used for $\rho_{w\pm}$ when performing the numerical integration in the integral equations corresponding to Eq. (32). In this step, we have used a fast algorithm for the exponential integral $E_1(x) = \int_x^\infty (1/t)\exp(-t)\mathrm{d}t$ provided by J. Jin (see http://jin.ece.uiuc.edu/routines/routines.html).

Table 5 Values of $\alpha(h)$ at $x_1 = 0.2$ at a large t ($t = 2000$) for the non-symmetric initial condition.

$-\alpha(h)$ $(d = 1,\ x_1 = 0.2,\ t = 2000)$				
$h = W$	$h = \|\Delta f\|^{(1)}$	$h = \rho$	$h = u_1$	$h = T$
1.000148	1.000487	2.014651	3.035255	0.997015

7 Concluding remarks

In the present study, we have investigated numerically the unsteady behavior of a free-molecular (or Knudsen) gas contained in a vessel with a uniform and constant temperature with special interest in the rate of approach to the final equilibrium state at rest. We assumed diffuse reflection as the boundary condition on the vessel wall and restricted ourselves to a vessel of spherical shape of dimension d, i.e., a sphere for the 3D case, a circular cylinder for the 2D case, and a gap between two parallel plates for the 1D case. Then, we mainly considered the spherically symmetric case assuming the initial condition to be the uniform equilibrium state at rest with a different temperature from the vessel wall. Such restrictions have made the computation for the 2D and 3D cases tractable. We have investigated the rate of approach to the final equilibrium state for the velocity distribution function as well as for the macroscopic quantities. The numerical results give evidence that the approach is slow and in proportion to an inverse power of time as given by Eq. (2). This conclusion is also supported by additional computations using a non-uniform initial condition in the 1D case.

We should note again that the initial conditions employed in the present numerical investigation are mild functions without the concentration of mass at zero molecular velocity. For extreme initial conditions with the mass concentrated near $\zeta_i = 0$ in a manner compatible with the relative entropy bound, one may have a different decay rate. On the contrary, we can consider a model system that does not contain low-speed molecules [for instance, the free transport equation (7) with an initial condition without slow molecules and a boundary condition that does not produce slow molecules]. In this case, one may expect a fast (perhaps exponential) approach to the final steady state, which is in general not an equilibrium state. Finally, if the so-called Maxwell-type boundary condition [i.e., $\alpha_{\rm ac} \times$ (diffuse reflection) + $(1 - \alpha_{\rm ac}) \times$ (specular reflection), where $\alpha_{\rm ac}$ is the accommodation coefficient] is assumed in place of diffuse reflection in the present problem, the same result as (2) is likely to hold with a larger value of $C^{(d)}$, unless the coefficient $\alpha_{\rm ac}$ is not small.

Acknowledgements The authors thank Laurent Desvillettes for valuable discussions. This work is supported by the grant-in-aid for scientific research No. 20360046 from JSPS.

References

1. Desvillettes, L.: Convergence to equilibrium in large time for Boltzmann and B.G.K. equations. Arch. Rational Mech. Anal., **110**, 73–91 (1990).
2. Lions, P.-L.: Compactness in Boltzmann's equation via Fourier integral operators and applications. I. J. Math. Kyoto Univ., **34**, 391–427 (1994).
3. Arkeryd, L., Nouri, A.: Boltzmann asymptotics with diffuse reflection boundary conditions. Mh. Math., **123**, 285–298 (1997).
4. Villani, C.: A review of mathematical topics in collisional kinetic theory. In: Friedlander, S., Serre, D. (eds.) Handbook of Mathematical Fluid Dynamics, vol. 1, pp. 71–305. Elsevier, Amsterdam (2002).
5. Desvillettes, L., Villani, C.: On the trend to global equilibrium for spatially inhomogeneous kinetic systems: The Boltzmann equation. Invent. Math., **159**, 245–316 (2005).
6. Villani, C.: Convergence to equilibrium: Entropy production and hypocoercivity. In: Capitelli, M. (ed.) Rarefied Gas Dynamics, pp. 8–25. AIP, Melville (2005).
7. Mouhot, C., Neumann, L.: Quantitative perturbative study of convergence to equilibrium for collisional kinetic models in the torus. Nonlinearity, **19**, 969–998 (2006).
8. Villani, C.: Hypocoercivity. Mem. Amer. Math. Soc., **202**, No. 950 (2009).
9. Guo, Y.: Decay and continuity of the Boltzmann equation in bounded domains. Arch. Rational Mech. Anal., published online (2009).
10. Ukai, S.: On the existence of global solutions of mixed problem for non-linear Boltzmann equation. Proc. Japan Acad. **50**, 179–184 (1974).
11. Caflisch, R. E.: The Boltzmann equation with a soft potential. II. nonlinear, spatially–periodic. Commun. Math. Phys. **74**, 97–109 (1980).
12. Lebowitz, J. L., Frisch, H. L.: Model of nonequilibrium ensemble: Knudsen gas. Phys. Rev., **107**, 917–923 (1957).
13. Arkeryd, L., Ianiro, N., Triolo, L.: The trend to a stationary state for the Lebowitz stick model. Math. Methods App. Sci., **16**, 739–757 (1993).
14. Bose, C., Grzegorczyk, P., Illner, R.: Asymptotic behavior of one-dimensional discrete-velocity models in a slab. Arch. Rational Mech. Anal., **127**, 337–360 (1994).
15. Yu, S.-H.: Stochastic formulation for the initial-boundary value problems of the Boltzmann equation. Arch. Rational Mech. Anal., **192**, 217–274 (2009).
16. Desvillettes, L., Salvarani, S.: Asymptotic behavior of degenerate linear transport equations. Bull. Sci. Math., **133**, 848–858 (2009).
17. Callen, H. B.: Thermodynamics, Chap. 6, Sec. 6.1. John Wiley and Sons, New York (1960).
18. Feller, W.: On the integral equation of renewal theory. Ann. Math. Stat., **12**, 243–267 (1941).
19. Feller, W.: An Introduction to Probability Theory and Its Applications, 2nd ed., Vol. 2, Chap. XI. John Wiley and Sons, New York (1971).
20. Babovsky, H.: On Knudsen flows within thin tubes. J. Stat. Phys., **44**, 865–878 (1986).
21. Babovsky, H., Bardos, C., Platkowski, T.: Diffusion approximation for a Knudsen gas in a thin domain with accommodation on the boundary. Asymptotic Anal., **3**, 265–289 (1991).
22. Golse, F.: Anomalous diffusion limit for the Knudsen gas. Asymptotic Anal., **17**, 1–12 (1998).
23. Caprino, S., Marchioro, C., Pulvirenti, M.: Approach to equilibrium in a microscopic model of friction. Commun. Math. Phys., **264**, 167–189 (2006).
24. Caprino, S., Cavallaro, G., Marchioro, C.: On a microscopic model of viscous friction. Math. Models Methods Appl. Sci., **17**, 1369–1403 (2007).
25. Aoki, K., Cavallaro, G., Marchioro, C., Pulvirenti, M.: On the motion of a body in thermal equilibrium immersed in a perfect gas. Math. Model. Num. Anal., **42**, 263–275 (2008).
26. Aoki, K., Tsuji, T., Cavallaro, G.: Approach to steady motion of a plate moving in a free-molecular gas under a constant external force. Phys. Rev. E., **80**, 016309 (2009).